

Thin Film Growth of 3D Sr-based Metal-Organic Framework on Conductive Glass via Electrochemical Deposition

Muhammad Usman,^[a] An-Chih Yang,^[b] Arif I. Inamdar,^[a] Saqib Kamal,^[a] Ji-Chiang Hsu,^[a, c] Dun-Yen Kang,^[b] Tien-Wen Tseng,^[c] Chen-Hsiung Hung,^{*[a]} and Kuang-Lieh Lu^{*[a, d]}

Integration of metal-organic frameworks (MOFs) as components of advanced electronic devices is at a very early phase of development and the fundamental issues related to their crystal growth on conductive substrate need to be addressed. Herein, we report on the structural characterization of a newly synthesized Sr-based MOF $\{[\text{Sr}(2,5\text{-Pzdc})(\text{H}_2\text{O})_2] \cdot 3\text{H}_2\text{O}\}_n$ (**1**) and the uniform crystal growth of compound **1** on a conducting glass (fluorine doped tin oxide (FTO)) substrate using electrochemical deposition techniques. The Sr-based MOF **1** was synthesized by the reaction of $\text{Sr}(\text{NO}_3)_2$ with 2,5-pyrazinedicar-

boxylic acid dihydrate (2,5-Pzdc) under solvothermal conditions. A single-crystal X-ray diffraction analysis revealed that **1** has a 3D structure and crystallizes in the triclinic $P\bar{1}$ space group. In addition, the uniform crystal growth of this MOF on a conducting glass (FTO) substrate was successfully achieved using electrochemical deposition techniques. Only a handful of MOFs have been reported to grown on conductive surfaces, which makes this study an important focal point for future research on the applications of MOF-based devices in microelectronics.

Introduction

Since the introduction of the structural chemistry of metal-organic frameworks (MOFs) at the end of the 20th century, tremendous research has been done on the fundamental properties of MOFs for various industrial devices particularly as sensors, in biomedicine, optoelectronic device, microelectronic circuits etc.^[1–3] However, in order to implement these functional materials into practical applications, it is of prime importance to design their relevant active devices or circuits using variety of substrates.^[4,5] These devices need to be highly stable, mechanically strong and highly efficient, meeting the requirement of recent trends in the technologies such as nanoscale fabrication

etc.^[6,7] In contrast to the traditional materials, the integration of MOFs into thin films faces significant challenges, for example, relatively low thermal and mechanical stabilities, less compatibility with inorganic or organic counterparts and the deposition of MOFs on variety of substrates.^[8] Furthermore, MOFs are generally known to be insulating materials and their deposition as a uniform thin film on conducting substrate is key factor for their applications in the areas of optoelectronics and microelectronics, especially in case of dielectrics, capacitors, transistors, DRAM and LEDs etc.^[5,9–11] Uniform growth of MOFs on a substrate plays a significant role in the measurement of charge transport properties of MOFs.^[11] Following the continuous progress in designing MOF films, significant efforts have been made to grow MOFs on diverse substrates.^[8,12]

Due to the wide variety of applicative measures of thin film of MOFs, different deposition methodologies are employed when different kinds of substrates are being used such as alumina, silicon wafers, Ag/Au nanosheets, copper foil, and glass slides.^[12–17] These reported methods are only successful for the deposition of MOFs on specific type of surface-modified and non-conducting substrates.^[18–20] To utilize MOFs in optoelectronic and microelectronic circuits, it is usually necessary to grow MOFs on conducting substrate such as transparent conducting oxide (TCO), F-doped SnO_2 or Sn-doped In_2O_3 (ITO), Cu, and carbon surfaces. Researchers have developed several techniques which demonstrated electrochemical deposition of various conducting materials into porous MOFs thin films, fabricated on conductive substrates.^[21–24]

During past few years, different deposition techniques such as anodic, cathodic and electrophoretic deposition have been applied for use in conjunction with their applications as supercapacitor, sensing, catalysis and separations etc.^[25,26] An lanthanide MOF thin film was reported to be electrodeposited by cathodic electrodeposition by applying voltage in a nitrate based electrolyte and the hydrolysis of benzophenone-3,3',4,4'-tetracarboxylic dia-


[a] Dr. M. Usman, Dr. A. I. Inamdar, Dr. S. Kamal, J.-C. Hsu, Prof. C.-H. Hung, Prof. K.-L. Lu
Institute of Chemistry
Academia Sinica
Taipei 115 (Taiwan)
E-mail: chhung@gate.sinica.edu.tw

[b] A.-C. Yang, Prof. D.-Y. Kang
Department of Chemical Engineering
National Taiwan University
Taipei 106 (Taiwan)

[c] J.-C. Hsu, Prof. T.-W. Tseng
Department of Chemical Engineering and Biotechnology
National Taipei University of Technology
Taipei 106 (Taiwan)

[d] Prof. K.-L. Lu
Department of Chemistry
Fu Jen Catholic University
New Taipei City 242 (Taiwan)
E-mail: kllu@gate.sinica.edu.tw

 Supporting information for this article is available on the WWW under <https://doi.org/10.1002/open.202100295>

 © 2022 The Authors. Published by Wiley-VCH GmbH. This is an open access article under the terms of the Creative Commons Attribution Non-Commercial NoDerivs License, which permits use and distribution in any medium, provided the original work is properly cited, the use is non-commercial and no modifications or adaptations are made.

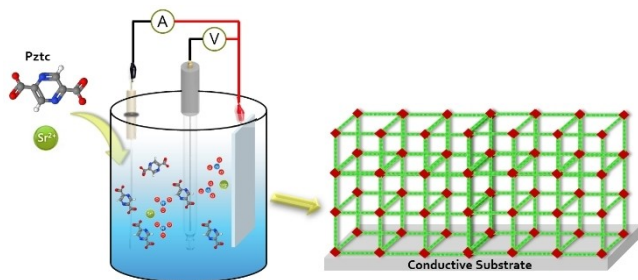
hydride, which resulted in the uniform direct deposition of MOFs on a conducting surface.^[27] Anodization techniques were also reported for the electrochemical synthesis of several MOFs including $\text{Cu}_3(\text{HHTP})_2$ on transparent conducting substrates for potential applications in optoelectronics as well as thermoelectrics.^[4,28] The concentration of linkers and metal ions plays an important role in controlling the thickness of films. In 2019, Nakamura et al. reported on the design of an electrochemically self-assembled Zn-based MOF, where the thickness is highly dependent on the concentration of the linker and with a lower concentrated oxidation process started at the electrode which can stop the further growth.^[29] However, Tang and co-workers simplified this into a two-step electrochemical deposition process for HKUST-1, which involves the electro-deposition of Cu on the substrate followed by the electro-oxidation of the Cu/ITO to MOF/ITO.^[30] Such controlled growth of MOFs on conductive substrate can be beneficial in term of expanding the applications of MOFs in the electronics industry.^[11,31]

The framing of suitable electrochemically deposition parameters allows variable functional MOFs to directly penetrate into conductive substrates and also provides a free hand for the tuning of homogeneity as well as surface topology so as to achieve the desired application.^[26] The electrochemical deposition of MOFs have previously been reported mostly for lanthanide and transition metals such as Zn, Cu, and Co etc. and the reports on alkaline-earth based MOFs (e.g. Mg, Ca and Sr etc.) are very limited.^[26,32] Herein, we report on the electrochemical deposition of strontium based MOF on conducting glass (fluorine doped tin oxide (FTO)) substrates by the reaction of strontium (Sr) ions and 2,5-pyrazinedicarboxylic acid dihydrate (2,5-Pzdc) (Scheme 1). Strontium has emerged as a significant component for the synthesis of luminescent and dielectric materials for micro- and optoelectronic devices.^[33,34] The growth of an Sr-based MOF on the surface of conducting substrates via electrochemical deposition will pave the way for their practical applications in electronic circuit design.

Results and Discussion

Synthesis of Sr-based MOF

Strontium-based materials have recently been used widely in the semiconductor industry because of their thermal stability,



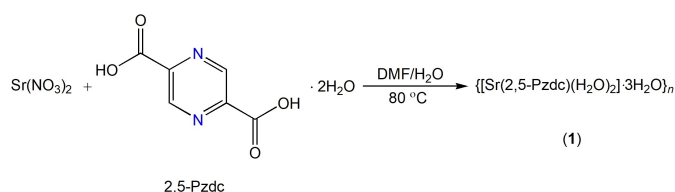
Scheme 1. Diagram demonstrating the systematic electrochemical growth of thin film of metal-organic framework on conductive substrates.

high reactivity and good mechanical strength.^[33,34] However, the thin film growth of these strontium-based MOFs has not been reported. Based on the distinction of strontium compounds, square shaped single crystals of compound $\{[\text{Sr}(2,5\text{-Pzdc})(\text{H}_2\text{O})_2] \cdot 3\text{H}_2\text{O}\}_n$ (**1**) were synthesized by reacting $\text{Sr}(\text{NO}_3)_2$ and 2,5-pyrazinedicarboxylate (2,5-Pzdc) in an DMF– H_2O solution under solvothermal conditions at 80°C for 3 days (Scheme 2). Fourier-transform infrared spectroscopic (FTIR) spectra confirmed the coordination of metal ions with the organic linker (2,5-Pzdc) as it shows a shift in peaks as well as addition of new peaks (e.g. $\nu=1690$ and 995 cm^{-1} etc.) as compared with free linker (Figure S1 in Supporting Information). The single-crystal data for compound **1** are shown in Table S1 and the powder X-ray pattern at room temperature is shown in Figure S2.

Crystal Structure of the Sr-based MOF

A single-crystal X-ray diffraction analysis revealed that **1** displays a 3D structure and crystallizes in the triclinic $P\bar{1}$ space group (Table S1). CCDC 2106396 contains the crystallographic data for this compound. The asymmetric unit consists of two strontium ions, two 2,5-Pzdc ligands and four coordinated water molecules as well as six guest H_2O molecules. The Sr(II) ions adopted two different coordination modes (Figure S3). The Sr(1) atom adopts a nine-coordinated geometry by two oxygen atoms (O_{10} , O_{11}) from the coordinated H_2O molecule, two nitrogen atoms (N_1 , N_2) from the azide group of ligands and five oxygen atoms (O_1 , O_3 , O_5 , O_9 and O_{14}) of carboxylic groups of 2,5-Pzdc ligands. Sr(2) atom shows nine-coordinated by two oxygen atoms (O_{12} , O_{13}) from coordinated H_2O , two nitrogen atoms (N_3 , N_4) from azide group and five oxygen atoms (O_3 , O_5 , O_7 , O_9 and O_{14}) from carboxylate groups of 2,5-Pzdc ligands (Figure 1).

The 2,5-Pzdc ligands are in a parallel arrangement and their carboxylate groups act as a bridge connecting Sr1 and Sr2 to form a metal-oxygen (Sr–O) chain along the y-axis (Figure 1c). These chains are interconnected via 2,5-Pzdc ligands to further expand the structure into three dimensions along the x-axis, leading to the formation and confirmation of a nanoporous three-dimensional structure, which is heavily occupied by guest solvent molecules, thus making the framework less porous (Figure 1b). Figure S3 shows a space filling model of **1** with maximum pore dimensions of $4.3 \times 7.4 \text{ \AA}$. These guest solvent (H_2O) molecules are stabilized in the pore of **1** through weak hydrogen bonding interactions. A topology analysis indicates that **1** (Figure 1d) possesses a 4,4 connected net, where the



Scheme 2. Synthesis of compound **1**.

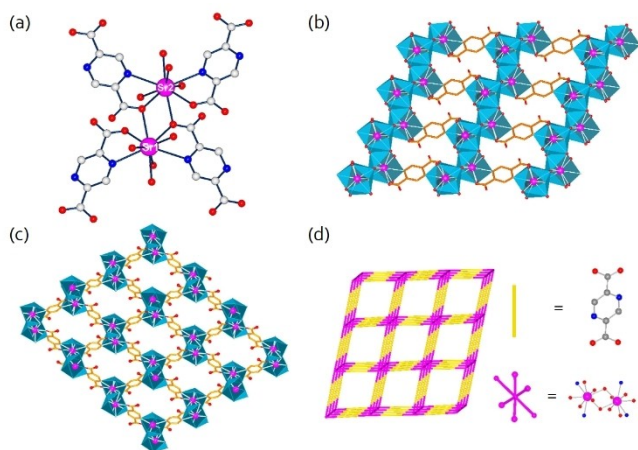


Figure 1. (a) The asymmetric building unit of the Sr-based MOF (1), in which Sr cations (M) with eight-coordinates and nine-coordinated modes are connected via 2,5-Pzdc linkers. (b) Polyhedral representation of metal-oxide layers connected via bridging organic linkers along the y-axis. (c) Crystal structure of 1, connected by the metal nodes and organic linkers to form hexagonal three-dimensional structure. (d) The structure of 1 adopts a (4,4) net topology.

Pzdc ligand functions as a two-connecting node and the Sr(II) metal ions act as a four-connecting node for both metal ions.

Powder X-ray diffraction patterns for 1 at room temperature indicate the phase purity of the MOF. From Figure S2, it can be observed that all of the PXRD peaks for the as-synthesized compound of 1 are closely matched with their corresponding PXRD peaks as attained via a simulated study of the structural data (cif) of 1 (CCDC 2106396). Diversity in the intensities of some peaks in the simulated and experimental results is due to the orientation preference of the powder samples, which is commonly observed in powder samples.

Electrochemical Deposition of Sr-MOF

The electrochemical deposition of Sr-based MOF was observed on an FTO substrate in a potential window 2 V to -2 V. For a better control and measurement of the current and potential passing through the cell during the electricity driven chemical reaction, a three-electrode setup was used in the electrochemical formation of the MOFs. With the assistance of a reference electrode (Ag/AgCl) with 0.1 M $[(n\text{-Bu}_4\text{N})\text{PF}_6]/\text{ACN}$ as a supporting electrolyte, the potential difference between the working and reference electrodes was precisely measured. Sr-MOF thin films were formed from the coordination of strontium ions with deprotonated organic ligands on the working electrode surface, which is fluorine-doped SnO (FTO) (Figure 2a).

Surface treatment of the FTO substrates has been carried out (as described in experimental section) before the deposition of any film to ensure complete removal of any surface impurities. The procedure was used for the deposition involved dissolving $\text{Sr}(\text{NO}_3)_2$ and 2,5-Pzdc in a DMF/ H_2O solvent mixture and immersing an FTO glass slide (as an electrode) in this precursor. The steady-state current during the electrodeposition

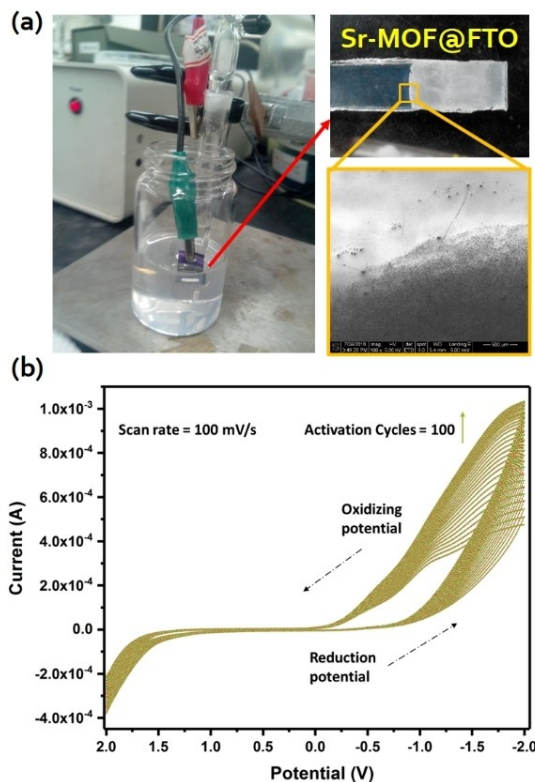


Figure 2. (a) Experimental setup used for the electrochemical deposition of Sr-based MOF on FTO glass. Optical image showing the MOF micro-sized crystals anchored on an FTO glass substrate (interface between deposition (solution dipped) of non-deposition area (solution undipped) is highlighted). (b) Evolution of the CV curves of a Sr-based MOF (1) thin film sample subject to the 100 cycles at a scan rate.

reached a value of -9×10^{-4} A under these conditions (Figure 2b). Instead of using the traditional method of secondary layer deposition of metal cations from the corrosion of the anode (metal enriched surface), we used a cathodic electro-deposition approach, where the electrochemical generation of hydroxide anions by the reduction of H_2O and NO_3^- cause the deprotonation of the 2,5-Pzdc ligand. The electrochemical generation of HO^- generates a pH gradient on the surface of the electrode, which assists in the deposition of strontium ions. The deprotonated ligands combine with metal ions via electrostatic interactions to form metal-ligand coordination on the surface. After 8000s of electrolysis for 100 segments, the formation of Sr-MOF crystals on the surface of FTO can be visualized by the naked eye (Figure 2a). From the optical image of film, it can be seen that MOF has been deposited on all the regions of the FTO, immersed in solution of electrochemical cell. When the FTO substrate was immersed into the MOF precursor without running the CV scan, there was no formation of MOF crystals as seen in Figure S6, which confirms that MOF thin films were only electrodeposited on FTO glass rather than chemically grown.

To confirm the formation of a MOF on the FTO, the powder X-ray diffraction (PXRD) pattern of the film was recorded. As shown in Figure 3, most of the peaks such as $2\theta = 8.7, 10.0, 11.7$ and 16.52° match well with the simulated and experimental

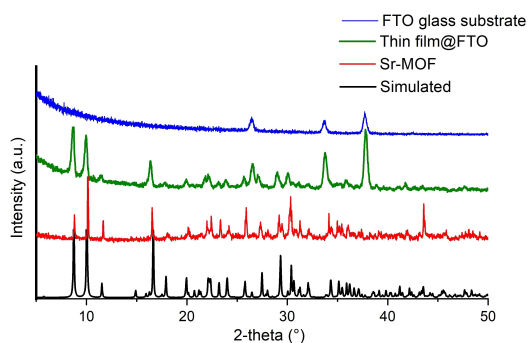


Figure 3. Powder X-ray diffraction patterns of the simulated data for **1** (black), as-synthesized compound **1** (red), thin film grown on the FTO substrate (green) and blank FTO substrate (blue).

PXRD patterns. However, the additional peaks $2\theta = 26.6$, 33.8 and 37.7° are representative peaks of the FTO.

Scanning electron microscopy (SEM) at different magnification scales (Figure 4) showed the uniform and highly concentrated crystal growth of MOFs on the surface of the FTO. The thickness and concentration of films are highly dependent on electrodeposition time used. As can be seen, increasing the time of electrodeposition from 25 to 130 minutes with 100 potential cycles resulted in a high concentration of MOFs being deposited on the substrate with the thickness in the range of (~ 1000 – 1500 nm). While with low potential cycles (50 and 20), the growth of MOFs on FTO is not uniform and the huge voids can be seen on the surface (Figure 4c & 4d). Since the concentration of metal and organic ligands is much higher at the bottom of electrochemical cell, the bottom edges of the FTO (completely

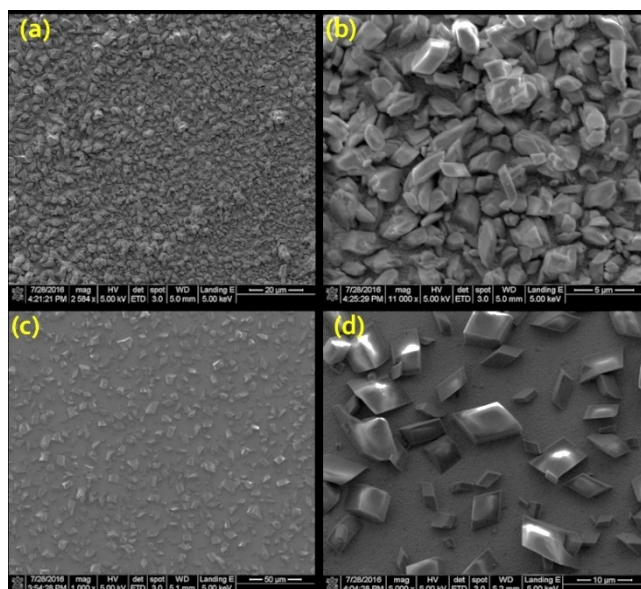


Figure 4. Scanning electron microscopic images after the electrochemical deposition of the Sr-based MOF on the FTO substrate for 100 potential cycles at (a) $2584\times$ ($20\ \mu\text{m}$ bar scale) and (b) $11000\times$ ($5\ \mu\text{m}$ bar scale) magnifications. SEM images of thin film deposition of **1** on FTO for (c) 50 potential cycles at $1000\times$ ($50\ \mu\text{m}$ scale bar) magnification and (d) 20 potential cycles at $5000\times$ ($10\ \mu\text{m}$ scale bar) magnification.

dipped in solution) have more surface covered as compared with the upper edges. The fabrication of such dense MOF films in such a short span of time (26.67 min) demonstrates the benefits of the electrochemical growth method as compared with other available surface deposition techniques which involves longer reaction times and higher temperatures etc. Furthermore, the self-assembly of MOF directly take place on conductive surface which gives more control for the fabrication of specific pattern during the electronic circuit design.

Conclusion

Herein, we have reported on the thin film growth of a newly synthesized three-dimensional Sr-based MOF via electrochemical deposition techniques in a three-cell setup. This is a rare case of thin film growth of a MOF, based on electrically felicitous strontium, on a conducting substrate (fluorine-doped SnO (FTO)). Scanning electron microscopic observations and a power X-ray diffraction analysis revealed that an electrochemical deposition for 100 potential cycles resulted in the uniform growth of a polycrystalline MOF layer on the conductive substrate. Fundamental thin film technique such as electrochemical deposition provides strong indications that MOFs as thin films will boost not only their use but also improve the efficiency of MOF based devices.

Experimental Section

Experimental Details

All the chemical reagents [$\text{Sr}(\text{NO}_3)_2$ (ACS reagent, $\geq 99.0\%$); 2,5-Pyrazinedicarboxylic acid dehydrate (96%) and N,N-dimethylformamide (DMF; $\geq 99.8\%$)] were purchased from commercial sources (Sigma-Aldrich) and were used as received without further purification. FTO substrates ($L\times W\times\text{thickness}$ $75\ \text{mm}\times 25\ \text{mm}\times 2\ \text{mm}$) were obtained from Thermo Fisher Scientific. Diffraction measurements for compound **1** were carried out using a Bruker-Nonius Kappa CCD diffractometer with graphite-monochromated $\text{Mo}_{K\alpha}$ radiation ($\lambda = 0.7107\ \text{\AA}$). Data collection parameters for compound **1** are listed in Table S1 (Supporting Information). The structure was solved using direct methods and refined using the SHELXL-97 program by full-matrix least-squares on F^2 values.^[35] All non-hydrogen atoms were refined anisotropically, whereas the hydrogen atoms were placed in ideal, calculated positions, with isotropic thermal parameters riding on their respective carbon atoms. Infrared spectra were recorded in the solid state (KBr pellets) on a Perkin-Elmer PARAGON 1000 FTIR spectrometer in the 4000 – $400\ \text{cm}^{-1}$ range. Powder diffraction data were recorded on a Siemens D-5000 diffractometer at 40 kV, 30 mA for $\text{Cu}_{K\alpha}$ ($\lambda = 1.5406\ \text{\AA}$), with a step size of 0.02° and scan speed of 1 s per step.

Deposition Number(s) 2106396 (**1**) contain(s) the supplementary crystallographic data for this paper. These data are provided free of charge by the joint Cambridge Crystallographic Data Centre and Fachinformationszentrum Karlsruhe Access Structures service www.ccdc.cam.ac.uk/structures.

Synthesis of MOFs

The Sr-MOF $\{[Sr_2(2,5\text{-Pzdc})_2(\text{H}_2\text{O})_2] \cdot 3\text{H}_2\text{O}\}_n$ (**1**) was synthesized using $\text{Sr}(\text{NO}_3)_2$ (10.6 mg, 0.05 mmol) and 2,5-pyrazinedicarboxylic acid (2,5-Pzdc) (10.2 mg, 0.05 mmol) as an organic linker in DMF:H₂O (2:4 mL) under solvothermal conditions at 80 °C for 72 h, which leads to the formation of transparent crystals. Colourless rectangular crystals of compound **1** were formed in 27.2% yield (based on Sr(II)). The solid product was separated by filtration and washed with water and dried at ambient temperature. IR (KBr): FTIR data (KBr, cm⁻¹): 3450(m), 3310(w), 3215(w), 3085(w), 2840(w), 2702(w), 2605(w), 2413(w), 1900(m), 1691(s), 1649(w), 1589(w), 1511(s), 1468(w), 1388(s), 1275(s), 1184(s), 1044(s), 995(m), 970(m), 793(s), 780(m), 620(s), 470(w).

Electrochemical Deposition Setup

Electrochemical disposition of MOF on fluorine doped tin oxide (FTO) glass substrates was performed via cyclic voltammetry method (CV) using CH instrument chemical analyser (CH1621B). A three-electrode electrochemical cell was used for the voltammetry measurements where Ag/AgCl was used as a reference electrode, platinum is a counter electrode and FTO was a working electrode. Glass substrates were placed in a cleaned beaker, added an appropriate amount of deionized water and detergent to the beaker, and then put them in an ultrasonic bath cleaner for 20 min. After this, the substrates were completely washed with deionized water, followed by second round of 20 min ultrasonic bath in a mixed solution of acetone, isopropanol, and deionized water. These substrates were finally washed again with excessive amount of deionized water and dried in a vacuum oven at 90 °C for one hour. Cleaned FTO glass was immersed in the solution containing MOF precursor. A precursor containing $\text{Sr}(\text{NO}_3)_2$ (31.8 mg, 0.15 mmol) and the organic linker 2,5-pyrazinedicarboxylate (Pzdc) (30.6 mg, 0.15 mmol) in DMF/H₂O (30 mL) was prepared and sonicated at room temperature for 12 h. The parallel mounted electrodes were immersed in approximately 30 mL of precursor solution. The electrostatics reactions on the FTO electrode resulted in the formation of a thin layer on the working electrode. The systematic diagram and real time optical image of the experimental setup is discussed above. Cyclic voltammetry was carried out at a sample scan rate 100 mV/s from 2 V to -2 V for 26.67 min (20 cycles). After repeating the experiments for different cycles ranging from 20 to 100 for 1600 to 8000 seconds, respectively, we obtained highly concentrated films of Sr-MOF on the FTO, which were washed and dried in air and then further analysed using SEM and PXRD.

Acknowledgements

We gratefully acknowledge Academia Sinica and Ministry of Science and Technology, Taiwan, for their financial support. We thank Dr. Yuh-Sheng Wen for solving and refining the crystal data.

Conflict of Interest

The authors declare no conflict of interest.

Data Availability Statement

The data that support the findings of this study are available in the supplementary material of this article.

Keywords: electrochemical deposition · metal-organic frameworks · microelectronics · strontium · thin film

- [1] H. Li, M. Eddaoudi, M. O'Keeffe, O. M. Yaghi, *Nature* **1999**, *402*, 276–279.
- [2] L. E. Kreno, K. Leong, O. K. Farha, M. Allendorf, R. P. Van Duyne, J. T. Hupp, *Chem. Rev.* **2012**, *112*, 1105–1125.
- [3] M. Usman, S. Mendiratta, K.-L. Lu, *Adv. Mater.* **2017**, *29*, 1605071.
- [4] R. Ameloot, L. Stappers, J. Fransaer, L. Alaerts, B. F. Sels, D. E. De Vos, *Chem. Mater.* **2009**, *21*, 2580–2582.
- [5] W.-J. Li, J. Liu, Z.-H. Sun, T.-F. Liu, J. Lü, S.-Y. Gao, C. He, R. Cao, J.-H. Luo, *Nat. Commun.* **2016**, *7*, 11830.
- [6] K. Ikigaki, K. Okada, Y. Tokudome, T. Toyao, P. Falcaro, C. J. Doonan, M. Takahashi, *Angew. Chem. Int. Ed.* **2019**, *58*, 6886–6890; *Angew. Chem.* **2019**, *131*, 6960–6964.
- [7] M.-S. Yao, J.-W. Xiu, Q.-Q. Huang, W.-H. Li, W.-W. Wu, A.-Q. Wu, L.-A. Cao, W.-H. Deng, G.-E. Wang, G. Xu, *Angew. Chem. Int. Ed.* **2019**, *58*, 14915–14919; *Angew. Chem.* **2019**, *131*, 15057–15061.
- [8] A. Bétard, R. A. Fischer, *Chem. Rev.* **2012**, *112*, 1055–1083.
- [9] M. Usman, S. Mendiratta, K.-L. Lu, *ChemElectroChem* **2015**, *2*, 786–788.
- [10] Z.-G. Gu, S.-C. Chen, W.-Q. Fu, Q. Zheng, J. Zhang, *ACS Appl. Mater. Interfaces* **2017**, *9*, 7259–7264.
- [11] X. Mu, W. Wang, C. Sun, J. Wang, C. Wang, M. Knez, *Adv. Mater. Interfaces* **2021**, *8*, 2002151.
- [12] D. Zacher, O. Shekha, C. Wöll, R. A. Fischer, *Chem. Soc. Rev.* **2009**, *38*, 1418–1429.
- [13] H. Ohara, S. Yamamoto, D. Kuzuhara, T. Koganezawa, H. Oikawa, M. Mitsuishi, *ACS Appl. Mater. Interfaces* **2020**, *12*, 50784–50792.
- [14] Q. Li, J. Gies, X.-J. Yu, Y. Gu, A. Terfort, M. Kind, *Chem. Eur. J.* **2020**, *26*, 5185–5189.
- [15] J. Warfsmann, B. Tokay, N. R. Champness, *Microporous Mesoporous Mater.* **2021**, *311*, 110686.
- [16] M.-Y. Kan, J. H. Shin, C.-T. Yang, C.-K. Chang, L.-W. Lee, B.-H. Chen, K.-L. Lu, J. S. Lee, L.-C. Lin, D.-Y. Kang, *Chem. Mater.* **2019**, *31*, 7666–7677.
- [17] D.-S. Chiou, H. J. Yu, T.-H. Hung, Q. Lyu, C.-K. Chang, J. S. Lee, L.-C. Lin, D.-Y. Kang, *Adv. Funct. Mater.* **2021**, *31*, 2006924.
- [18] J. Y. Kim, K. Barcus, S. M. Cohen, *J. Am. Chem. Soc.* **2021**, *143*, 3703–3706.
- [19] G. Delen, Z. Ristanović, L. D. B. Mandemaker, B. M. Weckhuysen, *Chem. Eur. J.* **2018**, *24*, 187–195.
- [20] T. Haraguchi, K. Otsubo, H. Kitagawa, *Eur. J. Inorg. Chem.* **2018**, *2018*, 1697–1706.
- [21] F. Wu, X. Guo, G. Hao, Y. Hu, W. Jiang, *Nanoscale* **2019**, *11*, 14785–14792.
- [22] C. Lu, T. Ben, S. Xu, S. Qiu, *Angew. Chem. Int. Ed.* **2014**, *53*, 6454–6458; *Angew. Chem.* **2014**, *126*, 6572–6576.
- [23] H. Yoo, A. Welle, W. Guo, J. Choi, E. Redel, *Nanotechnology* **2017**, *28*, 115605.
- [24] H. Al-Kutubi, J. Gascon, E. J. R. Sudhölter, L. Rassaei, *ChemElectroChem* **2015**, *2*, 462–474.
- [25] X. Zhang, K. Wan, P. Subramanian, M. Xu, J. Luo, J. Fransaer, *J. Mater. Chem. A* **2020**, *8*, 7569–7587.
- [26] H.-W. Jee, K.-J. Paeng, N. Myung, K. Rajeshwar, *ACS Appl. Electron. Mater.* **2020**, *2*, 1358–1364.
- [27] H. Liu, H. Wang, T. Chu, M. Yu, Y. Yang, *J. Mater. Chem. C* **2014**, *2*, 8683–8690.
- [28] M. de Lourdes Gonzalez-Juarez, E. Flores, M. Martin-Gonzalez, I. Nandhakumar, D. Bradshaw, *J. Mater. Chem. A* **2020**, *8*, 13197–13206.
- [29] T. Nakamura, S. Ueda, K. Uda, Y. Tsuda, Y. Hirai, H. Sun, T. Yoshida, *ECS Trans.* **2018**, *88*, 343–350.
- [30] L.-L. Jiang, X. Zeng, M. Li, M.-Q. Wang, T.-Y. Su, X.-C. Tian, J. Tang, *RSC Adv.* **2017**, *7*, 9316–9320.
- [31] J. Liu, C. Wöll, *Chem. Soc. Rev.* **2017**, *46*, 5730–5770.
- [32] X. Zhang, Y. Li, C. Van Goethem, K. Wan, W. Zhang, J. Luo, I. F. J. Vankelecom, J. Fransaer, *Matter* **2019**, *1*, 1285–1292.
- [33] G. Haider, M. Usman, T.-P. Chen, P. Perumal, K.-L. Lu, Y.-F. Chen, *ACS Nano* **2016**, *10*, 8366–8375.
- [34] P. Leo, D. Briones, J. A. García, J. Cepeda, G. Orcajo, G. Calleja, A. Rodríguez-Diéguez, F. Martínez, *Inorg. Chem.* **2020**, *59*, 18432–18443.
- [35] G. M. Sheldrick, *SHELX-97* **1997**.

Manuscript received: December 22, 2021

Revised manuscript received: January 16, 2022